Chalmers Publication Library

Mitigation of nonlinearities using conjugate data repetition

(article starts on next page)

Mitigation of nonlinearities using conjugate data repetition

Henrik Eliasson,[*] **Pontus Johannisson,**
Magnus Karlsson and Peter A. Andrekson

Photonics Laboratory, Department of Microtechnology and Nanoscience,
Chalmers University of Technology, SE-412 96, Gothenburg, Sweden

henrik.eliasson@chalmers.se

Abstract: We investigate a time-domain implementation of generalized phase-conjugated twin waves which we call conjugate data repetition. A theory based on time-domain perturbation analysis explaining the mitigation of nonlinear effects is provided, and the concept is evaluated using numerical simulations. Compared to PM-QPSK at the same channel bit rate, the single-channel transmission reach in a conventional system with standard single-mode fiber of conjugate data repetition-QPSK is increased by approximately a factor of 2.

References and links

1. E. Ip and J. M. Kahn, "Compensation of dispersion and nonlinear impairments using digital backpropagation," J. Lightwave Technology **26**, 3416–3425 (2008).
2. R. A. Fisher, B. R. Suydam, and D. Yevick, "Optical phase conjugation for time-domain undoing of dispersive self-phase-modulation effects," Opt. Lett. **8**, 611–613 (1983).
3. A. D. Shiner, M. Reimer, A. Borowiec, S. O. Gharan, J. Gaudette, P. Mehta, D. Charlton, K. Roberts, and M. O'Sullivan, "Demonstration of an 8-dimensional modulation format with reduced inter-channel nonlinearities in a polarization multiplexed coherent system," Opt. Express **22**, 20366–20374 (2014).
4. X. Liu, A. R. Chraplyvy, P. J. Winzer, R. W. Tkach, and S. Chandrasekhar, "Phase-conjugated twin waves for communication beyond the Kerr nonlinearity limit," Nat. Photonics **7**, 560–568 (2013).
5. X. Liu, S. Chandrasekhar, P. J. Winzer, R. W. Tkach, and A. R. Chraplyvy, "Fiber-nonlinearity-tolerant super-channel transmission via nonlinear noise squeezing and generalized phase-conjugated twin waves," J. Lightwave Technology **32**, 766–775 (2014).
6. X. Liu, S. Chandrasekhar, and P. Winzer, "Phase-conjugated twin waves and fiber nonlinearity compensation," in Optical Fibre Technology, OptoElectronics and Communication Conference and Australian Conference on Optical Fibre Technology (2014), pp. 938–940.
7. A. Ghazisaeidi, J. Renaudier, M. Salsi, P. Tran, G. Charlet, and S. Bigo, "System benefits of digital dispersion pre-compensation for non-dispersion-managed PDM-WDM transmission," in Proc. European Conference on Optical Communications (ECOC) (2013), p. We.4.D.4.
8. X. Liu, S. Chandrasekhar, A. H. Gnauck, P. J. Winzer, S. Randel, S. Corteselli, A. R. Chraplyvy, R. W. Tkach, B. Zhu, T. F. Taunay, and M. Fishteyn, "Digital coherent superposition for performance improvement of spatially multiplexed coherent optical OFDM superchannels," Opt. Express **20**, B595–B600 (2012).
9. X. Liu, S. Chandrasekhar, P. J. Winzer, A. R. Chraplyvy, R. W. Tkach, B. Zhu, T. F. Taunay, M. Fishteyn, and D. J. DiGiovanni, "Scrambled coherent superposition for enhanced optical fiber communication in the nonlinear transmission regime," Opt. Express **20**, 19088–19095 (2012).
10. Y. Tian, Y.-K. Huang, S. Zhang, P. R. Prucnal, and T. Wang, "Demonstration of digital phase-sensitive boosting to extend signal reach for long-haul WDM systems using optical phase-conjugated copy," Opt. Express **21**, 5099–5106 (2013).
11. S. L. I. Olsson, B. Corcoran, C. Lundström, M. Sjödin, M. Karlsson, and P. A. Andrekson, "Phase-sensitive amplified optical link operating in the nonlinear transmission regime," in Proc. European Conference on Optical Communications (ECOC) (2012), p. Th.2.F.1.

12. B. Corcoran, S. L. I. Olsson, C. Lundström, M. Karlsson, and P. A. Andrekson, "Mitigation of nonlinear impairments on QPSK data in phase-sensitive amplified links," in Proc. European Conference on Optical Communications (ECOC) (2013), p. We.3.A.1.

13. H. Eliasson, S. L. I. Olsson, M. Karlsson, and P. A. Andrekson, "Comparison between coherent superposition in DSP and PSA for mitigation of nonlinearities in a single-span link," in Proc. European Conference on Optical Communications (ECOC) (2014), p. Mo.3.5.2.

14. S. L. I. Olsson, C. Lundström, M. Karlsson, and P. A. Andrekson, "Long-haul (3465 km) transmission of a 10 GBd QPSK signal with low noise phase-sensitive in-line amplification," in Proc. European Conference on Optical Communications (ECOC) (2014), p. PD.2.2.

15. X. Liu, H. Hu, S. Chandrasekhar, R. M. Jopson, A. H. Gnauck, M. Dinu, C. Xie, and P. J. Winzer, "Generation of 1.024-Tb/s Nyquist-WDM phase-conjugated twin vector waves by a polarization-insensitive optical parametric amplifier for fiber-nonlinearity-tolerant transmission." Opt. Express **22**, 6478–85 (2014).

16. T. Yoshida, T. Sugihara, K. Ishida, and T. Mizuochi, "Spectrally-efficient dual phase-conjugate twin waves with orthogonally multiplexed quadrature pulse-shaped signals," in Proc. Optical Fiber Communications Conference and Exhibition (OFC) (2014), p. M3C.6.

17. W.-R. Peng, T. Tsuritani, and I. Morita, "Digital nonlinear noise cancellation approach for long-haul optical transmission systems," in Proc. European Conference on Optical Communications (ECOC) (2013), p. Mo.3.D.2.

18. X. Liu, S. Chandrasekhar, P. Winzer, R. W. Tkach, and A. R. Chraplyvy, "406.6-Gb/s PDM-BPSK superchannel transmission over 12,800-km TWRS fiber via nonlinear noise squeezing," in Proc. Optical Fiber Communications Conference and Exhibition (OFC) (2013), p. PDP5B.10.

19. P. Johannisson, M. Sjödin, M. Karlsson, H. Wymeersch, E. Agrell, and P. A. Andrekson, "Modified constant modulus algorithm for polarization-switched QPSK," Opt. Express **19**, 7734–7741 (2011).

20. J. Fischer, S. Alreesh, R. Elschner, F. Frey, M. Nölle, and C. Schubert, "Bandwidth-variable transceivers based on 4d modulation formats for future flexible networks," in Optical Communication (ECOC 2013), 39th European Conference and Exhibition on (2013), p. Tu.3.C.1.

21. A. Mecozzi, C. B. Clausen, and M. Shtaif, "Analysis of intrachannel nonlinear effects in highly dispersed optical pulse transmission," Photon. Technol. Lett. **12**, 392–394 (2000).

22. P. Johannisson, "Nonlinear intrachannel distortion in high-speed optical transmission systems," Ph.D. thesis, Chalmers University of Technology (2006).

23. M. J. Ablowitz and T. Hirooka, "Resonant nonlinear intrachannel interactions in strongly dispersion-managed transmission systems," Opt. Lett. **25**, 1750–1752 (2000).

24. A. Mecozzi, M. Tabacchiera, F. Matera and M. Settembre, "Dispersion management in phase modulated optical transmission systems," in Proc. European Conference on Optical Communications (ECOC) (2010), p. Mo.2.C.2.

25. D. Wang and C. R. Menyuk, "Polarization evolution due to the Kerr nonlinearity and chromatic dispersion," J. Lightwave Technology **17**, 2520–2529 (1999).

1. Introduction

Advanced modern fiber optical communication systems utilize coherent receivers and modulation formats that encode information on both the phase and amplitude of the optical field. In long-haul coherent systems, the main limiting factors to transmission reach are amplified spontaneous emission noise from the optical amplifiers and nonlinear distortion due to the Kerr nonlinearity that is accumulated during propagation in the optical fiber. Since the nonlinear distortion increases with higher optical launch power, the improvement of the signal-to-noise ratio that can be achieved by increasing the optical power of the signal is limited. There are several techniques that address the issue of nonlinear distortions. Digital back-propagation is a method which offers high performance at the cost of high computational requirements [1]. Another method is mid-span spectral inversion, sometimes referred to as optical phase conjugation, where both dispersion and nonlinear effects are compensated for by phase conjugating the signal in the middle of the link [2]. There has also been research into the design of multi-dimensional modulation formats that minimize the inter-channel nonlinear distortion that is generated during propagation in the fiber [3]. Another method of mitigating nonlinear distortion is phase-conjugated twin waves (PCTW) [4–6]. The principle behind PCTW is to transmit a signal and a phase-conjugated copy of the signal on the orthogonal polarization using a symmetric dispersion map [7], which leads to correlated nonlinear distortions on the two waves. The correlated distortions can then be cancelled by linear superposition. In [5] this was shown to increase the transmission reach of PCTW-QPSK compared to PM-QPSK approximately by

a factor of 3 while sacrificing 50 % spectral efficiency (SE). One can also transmit the conjugated copy in other signaling dimensions than polarization, for example different cores of a multi-core fiber [8, 9] or different wavelengths [10]. Systems that transmit the conjugated copy on a separate wavelength and mitigate nonlinear effects by all-optical coherent superposition in phase-sensitive amplifiers have been investigated both in single-span [11–13] and multi-span [14] transmission. The concept has also been demonstrated with phase conjugation of an entire WDM spectrum [15] and with diplexed twin waves in an effort to increase SE [16]. A time-domain approach called nonlinear noise cancellation has also been investigated in an orthogonal frequency division multiplexing system [17] and in [4] the connection between PCTW and nonlinear noise squeezing [18] was investigated. The increased complexity of the digital signal processing (DSP) due to the use of PCTW is minimal assuming that dispersion can be pre-compensated at the transmitter. The major drawback of PCTW is that the SE is decreased by a factor of two, i.e. requiring double symbol rate at the same bit rate.

In this paper we investigate an implementation of a generalized PCTW concept [5], which we call *conjugate data repetition* (CDR). When using CDR, the conjugated copy of the signal is transmitted in different time slots than the signal which brings several advantages. For example it is possible to use the conventional constant modulus algorithm (CMA) for adaptive channel equalization. For a PCTW quadrature phase shift keying (QPSK) signal this is not possible since it occupies two points on the Poincare sphere compared to four points with polarization-multiplexed (PM)-QPSK or CDR-QPSK which is required by the conventional CMA [19]. When discussing the possibility to use the conventional CMA it should be noted that the vector PCTW approach demonstrated in [15] also is compatible with the conventional CMA since the signals on the X- and Y-polarization at any given channel wavelength are uncorrelated. Another advantage is that the two polarizations of a PM-CDR-QPSK signal can be treated independently of each other in the DSP after polarization demultiplexing. A consequence of this is that implementation of CDR in existing PM-QPSK hardware could be easier than implementation of PCTW.

We provide a theoretical explanation for the mitigation of nonlinear distortions and investigate CDR by numerical simulations. Previously a theoretical explanation has been provided for the case of transmitting a signal and its conjugated copy on orthogonal polarizations [4]. However, the previously given theory is not valid for CDR, which is why we use a time-domain perturbation analysis to describe this case. We also compare in simulations the maximum transmission distance of CDR-QPSK to PM-QPSK and PCTW-QPSK at the same channel bit rate, 112 Gbit/s, for both single channel and wavelength division multiplexing (WDM) systems. The single channel transmission reach of CDR-QPSK compared to PM-QPSK at the same channel bit rate is increased by approximately a factor of two. This can be compared to using PM-BPSK which has the same SE as CDR-QPSK but increases the transmission reach by approximately a factor of two at the same symbol rate [20]. 16-ary quadrature amplitude modulation (16QAM) is also investigated in the single-channel case in an effort to use CDR at the same SE as PM-QPSK. An interesting result from the simulations is that the optimal dispersion map found by system simulations with inline ASE noise added differs slightly from the antisymmetric one predicted by the first order perturbation analysis.

2. Conjugate data repetition

The concept of CDR is visualized in Fig. 1. A conjugated pulse copy, a_N^*, of each signal pulse, a_N, is transmitted in the consecutive pulse slot and a linear superposition C_N of the two pulses making up a supersymbol is done in the receiver DSP according to
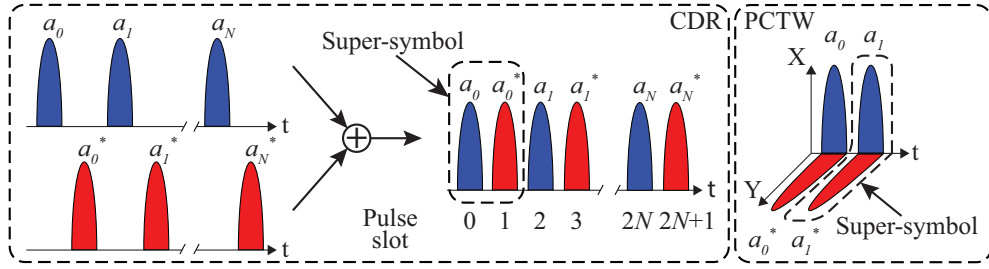
$$C_N = a_N + (a_N^*)^*, \tag{1}$$

Fig. 1. The transmitted signal for CDR and PCTW. For CDR, a conjugated copy S_N^* of each signal symbol S_N is transmitted in the consecutive pulse slot. Also shown in the figure is the numbering of pulses used to specify pulse triplets in the perturbation analysis of Section 2.1.

where N is the super-symbol index. As for PCTW, the concept can be viewed as applying a rate $1/2$, length 2 symbols inner code that repeats all symbols conjugated. Over an additive white Gaussian noise channel, the choice of conjugating the repeated symbol instead of repeating the same symbol twice will not change performance. However, as will be shown, using a antisymmetric dispersion map and a symmetric powermap over a link without dispersion compensation and coherently superposing the received symbols in the receiver DSP will lead to mitigation of nonlinear distortion in a similar way as for PCTW.

2.1. Theory using time-domain perturbation analysis

It is possible to show that part of the nonlinear distortion is cancelled in the linear superposition shown in Eq. (1) when using CDR. In the following, a theoretical explanation for the mitigation of nonlinear distortion will be presented. The analysis is based on time-domain perturbation analysis [21]. The aim of the analysis is to find the nonlinear perturbation on the signal and conjugate pulses of super-symbol number 0 generated by different pulse triplets (k,l,m). When the perturbations have been calculated, it is possible to find corresponding pulse triplets which generate nonlinearities on the signal and conjugate pulses that cancel out in the superposition operation of Eq. (1). The governing model equation for scalar propagation in the fiber is the nonlinear Schrödinger equation

$$i\frac{\partial \psi}{\partial z} = \frac{\beta_2}{2}\frac{\partial^2 \psi}{\partial t^2} - i\frac{\alpha}{2}\psi - \gamma|\psi|^2\psi, \tag{2}$$

where $\psi = \psi_S + \psi_P$, ψ_S is the signal field and ψ_P is the field of the perturbation. The amplitude of the perturbation is assumed to be small compared to the amplitude of the signal and ψ_S is the solution to the linear propagation equation with $\gamma = 0$. The initial signal $\psi_S(0,t)$ is modeled as a train of Gaussian pulses according to

$$\psi_S(0,t) = \sum_k \left[a_k\psi_0(t-2kt_p) + a_k^*\psi_0(t-(2k+1)t_p)\right], \tag{3}$$

where $\psi_0(t) = \exp(-t^2/(2t_0^2))$ is the Gaussian pulse shape, t_p is the pulse slot duration and a_k are the complex-valued symbols. It can be shown that the perturbation generated by three pulses (k,l,m) to first order, i.e. assuming that the nonlinear perturbation ψ_P is generated by ψ_S alone, is [21, 22]
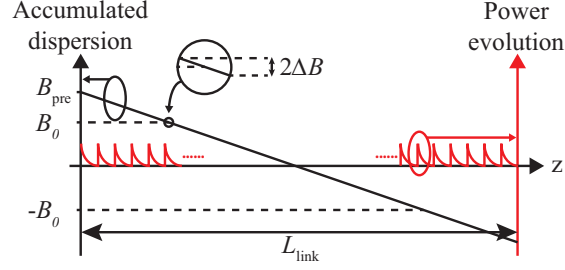
Fig. 2. The antisymmetric dispersion map used for CDR and PCTW. B_{pre} is the dispersion which is pre-compensated for, B_0 is an arbitrarily chosen accumulated dispersion where the perturbations are evaluated and $2\Delta B$ is a small interval around B_0 that sets the limits of the integrals of Eqs. (5) and (6). The red line shows how the optical power varies along the link.

$$\psi_{P,(k,l,m)}(L,t) = \qquad (4)$$

$$ia_k a_l a_m^* \int_0^L \frac{\gamma p(z)}{\sqrt{1 + 2iB + 3B^2}}$$

$$\exp\left(-\frac{1}{2}\frac{3+iB}{1+3iB}\left[\left(\frac{t}{t_0}\right)^2 - 2\frac{t}{t_0}\frac{(1+iB)(\tau_k+\tau_l)+(1-iB)\tau_m}{3+iB}\right]\right)$$

$$\exp\left(-\frac{1}{2}\frac{1}{1+B^2}\left[(\tau_k^2+\tau_l^2)(1+iB)+\tau_m^2(1-iB)-\right.\right.$$

$$\left.\left.\{(\tau_k+\tau_l)(1+iB)+\tau_m(1-iB)\}^2\frac{iB}{1+3iB}\right]\right)dz$$

where $B = B(z) = B_{pre} + (1/t_0^2)\int_0^z \beta_2(z')dz' = B_{\text{pre}} + z\beta_2/t_0^2$ is the accumulated dispersion and B_{pre} is due to dispersion pre-compensation. The center of pulse k is denoted by $\tau_k = kt_p/t_0$, and $p(z) = P(z)/P_0$ where $P(z)$ and P_0 are the local and initial values of the power, respectively. The expression in Eq. (4) is derived under the assumption that the accumulated dispersion is post-compensated to zero. We will, without loss of generality, consider the perturbation in the center of pulse slot 0, i.e. choose $t = 0$. By doing this, the first exponential function in Eq. (4) equals one. The next step is to approximate the integral. We assume that $B \gg 1$, which is fulfilled for most of the propagation, and in this limit some of the terms in the second exponential function can be neglected. Also, it can be shown that in the limit $B \gg 1$, the perturbation from three pulses (k,l,m) ends up in pulse slot $k+l-m$ [23], this will be used to find all pulse triplets that generate perturbations in pulse slots 0 and 1. In order to write the resulting equation on a compact form we make a change of variables from z to accumulated dispersion $B = B_{\text{pre}} + z\beta_2/t_0^2$. We will study the perturbation that is generated during propagation over a small interval $2\Delta B$ around an arbitrarily chosen B_0. By choosing $m = k+l$ we study the perturbation generated in pulse slot 0, i.e., on the signal pulse of super-symbol C_0, during propagation from $B_0 - \Delta B$ to $B_0 + \Delta B$ which is found as

$$\psi_{P,(k,l,k+l)}(B_0,0) = ia_k a_l a_{k+l}^* \int_{B_0-\Delta B}^{B_0+\Delta B} \frac{\gamma p(B)}{\sqrt{3}|B|} e^{i\frac{3v^2kl-1}{3B}}\frac{t_0^2}{\beta_2}dB, \qquad (5)$$

where $v = t_p/t_0$. The dispersion map together with the variables B_{pre}, B_0 and ΔB is illustrated in Fig. 2. By translating the pulse indices (k,l,m) by one step we find the perturbation generated

Table 1. Pulse triplets that generate perturbations on the signal and conjugate pulse of C_0 which cancel out after coherent superposition. Also shown is the form of the triplets fulfilling $k + l - m = 0$ for which it is not possible to find a corresponding triplet so that the nonlinear perturbations cancel. For suitable choices of the integers M and N, the first column includes all possible choices of triplets fulfilling $k + l - m = 0$.

Perturbation in	Pulse slot 0, signal pulse of C_0	Pulse slot 1, conjugate pulse of C_0
(k,l,m) for cancelling pulse triplets	$(2N, 2M, 2N+2M)$	$(2N+1, 2M+1, 2N+2M+1)$
	$(2N, 2M+1, 2N+2M+1)$	$(2N+1, 2M, 2N+2M)$
	$(2N+1, 2M, 2N+2M+1)$	$(2N, 2M+1, 2N+2M)$
(k,l,m) for non-cancelling pulse triplets	$(2N+1, 2M+1, 2N+2M+2)$	none

in pulse slot 1, the conjugate pulse of super-symbol C_0, during propagation from $B_0 - \Delta B$ to $B_0 + \Delta B$ by the pulse triplet $(k, l, k+l-1)$ to be

$$\psi_{P,(k,l,k+l-1)}(B_0, t_p) = i a_k a_l a_{k+l-1}^* \int_{B_0-\Delta B}^{B_0+\Delta B} \frac{\gamma p(B)}{\sqrt{3}|B|} e^{i \frac{3v^2(k-1)(l-1)-1}{3B}} \frac{t_0^2}{\beta_2} dB. \tag{6}$$

Using Eqs. (5) and (6) we can find triplets which generate perturbations that cancel out in the linear superposition operation of Eq. (1). The calculations for a specific pair of pulse triplets are shown in the Appendix. In these calculations we assume an antisymmetric dispersion map, $B(z) = -B(L_{\text{link}} - z)$, and a symmetric power map, $p(z) = p(L_{\text{link}} - z)$, where L_{link} is the total link length. These are the same assumptions regarding the power and dispersion map that was assumed in the derivation for PCTW [4]. We note that even though we simulate a system with EDFAs (Erbium-doped fibre amplifier), it is possible that the performance of CDR could be improved further by employing Raman amplification, since it is possible to achieve a power map which is closer to symmetric. There are also other choices of pulse triplets than the one shown in the Appendix for which it is possible to find cancelling triplets. Further, it is possible to find pulse triplets that generate distortion on the signal pulse of C_0 for which there is no corresponding triplet that generate distortion on the conjugate pulse of C_0 that cancel out in the superposition operation. The indices of both cancelling and non-cancelling triplets are summarized in Table 1. Even though there are nonlinear perturbations that are not cancelled according to the theory, we will see in Section 3.1 that CDR-QPSK performs similar to PCTW-QPSK. This is a surprising and, in our view, interesting observation since the perturbation analysis does not tell us how much better PCTW performs compared to CDR.

It is important to note that the above derivation is valid only in a highly dispersive regime where $|B| \gg 1$. As the analysis is not valid in an intermediate dispersion regime where $|B|$ is very small, it is possible that the mitigation of nonlinearities is less efficient in this regime.

The effects of matched filtering are excluded from this derivation in the same way as in [4]. Both the signal and the generated perturbation take the form of Gaussian pulses. However, since the perturbation pulses are products of three signal pulses, their spectrum will be slightly broader. A consequence of this is that part of the energy in the perturbation pulses will be lost in matched filtering.

3. Numerical simulations

Numerical simulations have been carried out to compare the transmission reach of CDR-QPSK and CDR-16QAM to that of PCTW-QPSK and PM-QPSK at the same channel bit rates. In order to have the same channel bit rate, the symbol rate of CDR-QPSK and PCTW-QPSK is

56 GBaud while the symbol rate of CDR-16QAM and PM-QPSK is 28 GBaud. For the CDR formats, two independent CDR symbol streams are transmitted on the X- and Y- polarization states. Simulations were performed to evaluate the performance of both single channel systems and WDM systems. In the case of WDM, the channel spacing was 50 GHz at 28 GBaud and 100 GHz at 56 GBaud. Assuming a channel data rate of 100 Gbit/s due to FEC overhead, the SE using PM-QPSK or CDR-16QAM is 2 bit/s/Hz and the SE using PCTW-QPSK or CDR-QPSK is 1 bit/s/Hz. Seven WDM channels were transmitted giving an aggregate data rate of 700 Gbit/s. The transmitter and LO lasers have a linewidth of 100 kHz. The transmitted optical signal is non-return-to-zero (NRZ) with a 5th order Bessel filter characteristic with FWHM bandwidth 75 % of the symbol rate. Note that the NRZ signal used in the simulations is different from the Gaussian pulses used in the perturbation analysis of Section 2.1. The resolution of the propagating waveforms are 32 samples per symbol and the number of symbols is 2^{17}. Before transmitting the signal, dispersion is digitally pre-compensated in the transmitter in order to obtain an antisymmetric dispersion map at the targeted number of spans, the span length is 80 km. For single channel CDR-QPSK and PCTW-QPSK the dispersion map is antisymmetric after 200 spans, 16,000 km and for WDM simulations the dispersion map is antisymmetric after 150 spans, 12,000 km. For PM-QPSK no dispersion pre-compensation is applied. We have two reasons for not optimizing the dispersion map for PM-QPSK. First, PM-QPSK without dispersion precompensation is a well studied and common implementation in commercial coherent PM-QPSK systems, making it a suitable choice as a baseline reference. Second, the optimization of dispersion maps for QPSK systems without inline dispersion compensation has been studied before [7, 24] and was shown to provide little benefit. For single-channel CDR-16QAM, the dispersion map is symmetric at 7,200 km, corresponding to the reach of PM-QPSK at BER $= 10^{-3}$. The waveform is propagated using the split-step Fourier method solution of the Manakov model [25, Eq. (1)]. The effects of polarization mode dispersion (PMD) are neglected but could be an interesting topic for further investigation. In previous investigations of PMD in a PCTW system, the worst case scenario due to PMD was improved by using PCTW [15]. The signal is propagated over dispersion-uncompensated 80 km spans of single-mode fiber (SMF) with dispersion parameter $D = 17$ ps/(nm km), loss $\alpha = 0.2$ dB/km and nonlinear coefficient $\gamma = 1.27$ W^{-1}km^{-1}. Fiber loss is compensated by inline erbium-doped fiber amplifiers with a noise figure (NF) of 5.5 dB. This does not provide a symmetric power map in contrast to the assumption of the perturbation analysis of Section 2.1.

The receiver DSP begins with downsampling to two samples per symbol. After that, the dispersion is post-compensated using electronic dispersion compensation. The equalization and polarization demultiplexing algorithms are different for the different modulation formats. For PM-QPSK and CDR-QPSK, the conventional CMA is used. For PCTW-QPSK, the conventional CMA cannot be used since the optical field of PCTW-QPSK occupies two points on the Poincare sphere compared to the four points of PM-QPSK and CDR-QPSK. Instead the polarization-switched CMA (PS-CMA) [19] is used for equalization of PCTW-QPSK. A decision-directed least mean square equalizer was used for CDR-16QAM. Phase synchronization is performed on the equalized symbols before coherently superposing the signal and conjugate pulses of a supersymbol in the case of CDR-QPSK, CDR-16QAM and PCTW-QPSK. The superposed symbols C_N are then used for BER counting. For PM-QPSK the BER counting is done directly after the phase tracking. In WDM simulations, only the BER of the center channel is counted. In all cases Gray-coded modulation is used.

3.1. Results

Single-channel simulation results with BER as a function of transmission distance are shown in Fig. 3a and WDM results in Fig. 3b, the BER as a function of launch power for single-channel
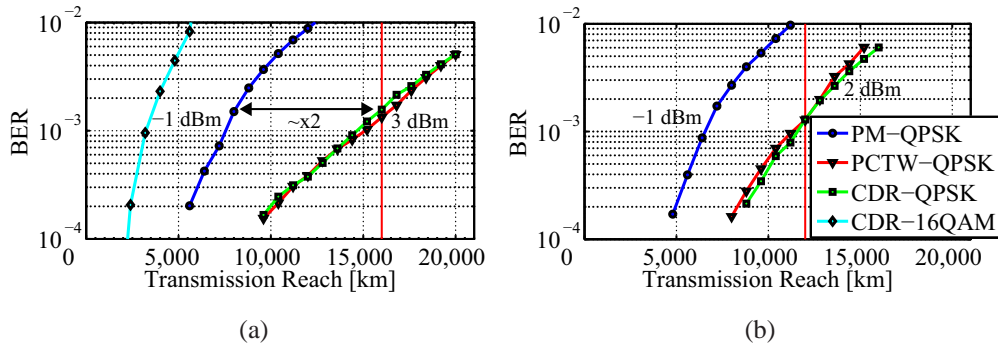
Fig. 3. Simulated BER as a function of transmission distance for (a) single channel and (b) 7-channel WDM for 28 GBaud PM-QPSK, 56 GBaud PCTW-QPSK, 56 GBaud CDR-QPSK and 28 GBaud CDR-16QAM. Optimum launch powers are specified in the figures. The distance where the dispersion map is perfectly symmetric is marked with a vertical red line.

PM-QPSK and CDR-QPSK is shown in Fig. 4. In the single-channel case the optimum launch power for PM-QPSK and CDR-16QAM was −1 dBm, for CDR- and PCTW-QPSK the optimum launch power was 3 dBm. In the WDM case, the optimum launch power for PM-QPSK was −1 dBm. For PCTW-QPSK and CDR-QPSK the optimum launch power was 2 dBm indicating that the mitigation of nonlinearities is less efficient in the WDM case, as expected. The transmission reaches are compared at the BER of CDR-QPSK at the distance where the dispersion map is symmetric, 16,000 km for single channel and 12,000 km for WDM. In the single channel case, the transmission reach of PM-QPSK is 8,000 km. The reach of CDR-QPSK is 16,000 km, i.e. an increase by approximately a factor of 2. The reach of PCTW-QPSK is 16,480 km, an increase by approximately a factor of 2.1. For WDM, the transmission reach of PM-QPSK is 6,800 km while the reach of CDR-QPSK and PCTW-QPSK is 12,000 km corresponding to an increase by a factor of 1.8. It is important to point out that we are propagating the signal in SMF. In previous demonstrations of PCTW, fibers with other parameters have been used that can give larger relative gains in transmission reach [5]. It is clear from the relative reach increase that the concept of CDR in the same way as channel-wise PCTW becomes less efficient in a WDM scenario because of inter-channel nonlinear effects. These results indicate very similar performance when comparing PCTW-QPSK to CDR-QPSK. In an effort to use the concept of CDR without sacrificing SE compared to PM-QPSK, a single-channel CDR-16QAM system was also simulated, the results from these simulations are shown in Fig. 3a. However it is clear that in the same way as for PCTW-16QAM [5], it is not possible to increase the transmission reach while maintaining SE.

Simulations were also performed to evaluate the performance of CDR-QPSK in a single-channel system with low-noise optical amplifiers with a 3-dB noise figure. For these simulations the dispersion map was symmetric at a distance of 23,200 km. The results from these simulations are shown in Fig. 5a. In this case, the transmission reach of PM-QPSK is 11,440 km while CDR-QPSK has a transmission reach of 23,200 km leading to approximately the same increase in transmission reach by a factor of 2. The impact of the dispersion map design was also studied by evaluating the system performance with dispersion maps that are not perfectly symmetric. The BER as a function of dispersion pre-compensation for single-channel 56 GBaud CDR-QPSK over a 16,000 km link is shown in Fig. 5b. Interestingly we see that the minimum BER is not at 50 % dispersion precompensation as the first-order theory of Section 2.1 predicts
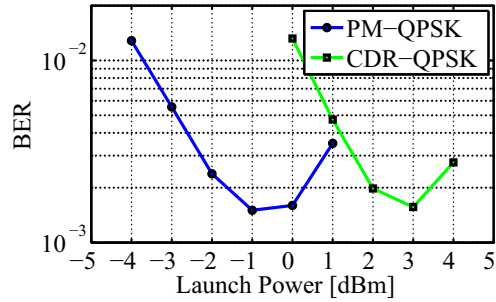
Fig. 4. The BER as a function of launch power for 28 GBaud PM-QPSK at 8,000 km (blue line) and 56 Gbaud CDR-QPSK at 16,000 km (green line).

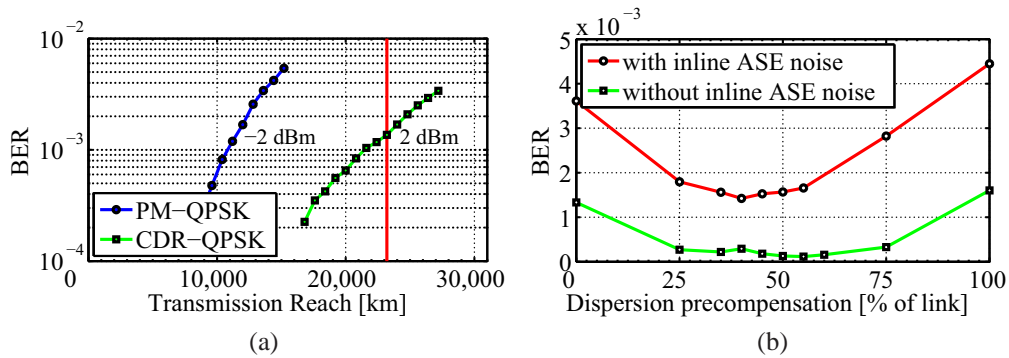(a)   (b)

Fig. 5. (a) The BER as a function of transmission distance for single channel 28 GBaud PM-QPSK and 56 GBaud CDR-QPSK in a system with 3 dB noise figure optical amplifiers. The optimum launch powers are specified in the figure and the distance where the dispersion map is symmetric is marked with a vertical red line. (b) The BER of single channel 56 GBaud CDR-QPSK as a function of dispersion pre-compensation with a link length of 16,000 km, with and without ASE noise added by inline amplifiers.

but at approximately 40 % dispersion precompensation. A possible explanation for this is that the signal-noise and higher-order nonlinear interactions become stronger the further the signal has propagated, leading to less efficient mitigation of nonlinear effects generated closer to the end of the link. In order to investigate this further we turned off the addition of ASE noise in the inline EDFAs. When running these simulations, the optimum point moved very close to 50 %. This indicates that the main reason behind 40 % being the optimum amount of dispersion pre-compensation in the CDR system is signal-noise interactions. However, the difference in performance is very small so that a perfectly symmetric dispersion map can be used with a negligible penalty.

4. Conclusion

We have demonstrated theoretically why it is possible to mitigate nonlinear effects using CDR. The analysis is based on a first order time-domain perturbation analysis and shows how the nonlinear perturbations from different pulse triplets cancel out after linear superposition when using a symmetric dispersion map. Simulations were performed to quantify the transmission reach of CDR-QPSK in comparison to PM-QPSK and PCTW-QPSK. At the same channel bit

rate, the transmission reach of CDR-QPSK is increased by a factor of 2 in a single channel system and by a factor of 1.8 in a WDM system when compared to PM-QPSK. With an effective length $L_{\text{eff}} = 21$ km, the total nonlinear phase shift $\Phi_{\text{NL}} = N_{\text{span}}L_{\text{eff}}P_{\text{launch}}\gamma = 2.1$ radians for the PM-QPSK system at 8,000 km and 10.7 radians for CDR-QPSK at 16,000 km showing an increased tolerance against nonlinear effects by more than a factor of five. The transmission reaches of PCTW-QPSK and CDR-QPSK are similar so it is hard to favor the use of CDR over PCTW from a performance perspective. However there are differences in the implementation of the two different formats which could make CDR attractive in some scenarios. One important difference is that the conventional CMA algorithm works for a CDR-QPSK signal while it will not work for a PCTW-QPSK signal. If CDR is used as a fallback solution in a PM-QPSK system using the conventional CMA algorithm for polarization demultiplexing and equalization, the equalizer could be run without modifications. We have also shown that in the same way as for PCTW, it is not possible to use CDR together with 16QAM to improve transmission reach at the same time as maintaining SE. It is also worth noting that we have demonstrated mitigation of nonlinearities even though the CDR signal is complex-valued, in contrast to the signal of PCTW which is real-valued under certain polarization rotations [4]. Finally we have shown in our simulations of a CDR-QPSK system that the optimal amount of dispersion precompensation differs from the 50 % predicted by the first-order theory. The simulations show that the optimal amount of dispersion pre-compensation is approximately 40 %, mainly due to signal noise interaction. However it is also important to note that the penalty caused by using 50 % dispersion pre-compensation instead of 40 % is very small.

Appendix: Perturbation analysis of a specific pair of pulse triplets

The following analysis shows that the perturbations generated by the triplets $(k,l,m) = (2N, 2M, 2N+2M)$ and $(k,l,m) = (2N+1, 2M+1, 2N+2M+1)$, where M and N are arbitrary integers, cancel out in the linear superposition of Eq. (1). The perturbations are evaluated at two points along the link with accumulated dispersion $\pm B_0$. According to Eq. (5), the perturbation generated in pulse slot 0, the signal pulse of super-symbol C_0, during propagation from $B_0 - \Delta B$ to $B_0 + \Delta B$, by the pulse triplet $(k,l,m) = (2N, 2M, 2N+2M)$ is

$$\psi_{P,(2N,2M,2N+2M)}(B_0, 0) =$$
$$ia_N a_M a_{N+M}^* \int_{B_0-\Delta B}^{B_0+\Delta B} \frac{\gamma p(B)}{\sqrt{3}|B|} e^{i\frac{12v^2 NM-1}{3B}} \frac{t_0^2}{\beta_2} dB = ia_N a_M a_{N+M}^* R_{2N,2M}, \quad (7)$$

where $R_{k,l}$ is the value of the integral. In the same way we can find the perturbation generated during propagation from $-B_0 - \Delta B$ to $-B_0 + \Delta B$ to be

$$\psi_{P,(2N,2M,2N+2M)}(-B_0, 0) = ia_N a_M a_{N+M}^* R_{2N,2M}^*, \quad (8)$$

since a change in the sign of B leads to conjugation of the value of the integral. Also in order for the integrals to be equal, we assume a symmetric power map, i.e. $p(B) = p(-B)$. Next, Eq. (6) is used to calculate the perturbation generated in pulse slot 1, i.e. the conjugate pulse of super-symbol C_0, by the pulse triplet $(k,l,m) = (2N+1, 2M+1, 2N+2M+1)$ during propagation between $B_0 - \Delta B$ and $B_0 + \Delta B$ to be

$$\psi_{P,(2N+1,2M+1,2N+2M+1)}(B_0, 0) =$$
$$ia_N^* a_M^* a_{N+M} \int_{B_0-\Delta B}^{B_0+\Delta B} \frac{\gamma p(B)}{\sqrt{3}|B|} e^{i\frac{12v^2 NM-1}{3B}} \frac{t_0^2}{\beta_2} dB = ia_N^* a_M^* a_{N+M} R_{2N,2M}, \quad (9)$$

and at negative B_0

$$\psi_{P,(2N+1,2M+1,2N+2M+1)}(-B_0, 0) = ia_N^* a_M^* a_{N+M} R_{2N,2M}^*. \quad (10)$$

If we do coherent superposition of the nonlinear perturbation terms according to Eq. (1) we get

$$
\begin{aligned}
&\psi_{P,(2N,2M,2N+2M)}(B_0,0) + \psi_{P,(2N,2M,2N+2M)}(-B_0,0) + \\
&\left(\psi_{P,(2N+1,2M+1,2N+2M+1)}(B_0,0) + \psi_{P,(2N+1,2M+1,2N+2M+1)}(-B_0,0)\right)^* = \\
&i a_N a_M a^*_{N+M} R_{2N,2M} + i a_N a_M a^*_{N+M} R^*_{2N,2M} + \\
&\left(i a^*_N a^*_M a_{N+M} R_{2N,2M} + i a^*_N a^*_M a_{N+M} R^*_{2N,2M}\right)^* = 0,
\end{aligned}
\tag{11}
$$

i.e., the perturbations cancel out in the superposition operation of Eq. (1).

Acknowledgments